Applied Surface Science 548 (2021) 149215

Contents lists available at ScienceDirect

Applied Surface Science

journal homepage: www.elsevier.com/locate/apsusc

Full Length Article

Induced magnetization in Cu atoms at the Fe-Co/Cu_3Au(001) interface: X-ray magnetic circular dichroism experiments and theoretical results

Sofia O. Parreiras [a,1,2], Luis A. Cabral [b,1], Rodrigo V. Lourenço [a], Alexandre A.C. Cotta [c], Pedro Schio [d], Julio C. Cezar [d], Pedro L. Gastelois [a], Edison Z. da Silva [b,*], Waldemar A. A. Macedo [a,*]

[a] Centro de Desenvolvimento da Tecnologia Nuclear, CDTN, 31270-901 Belo Horizonte, MG, Brazil
[b] Institute of Physics "Gleb Wataghin", University of Campinas-UNICAMP, 13083-859 Campinas, SP, Brazil
[c] Departmento de Física, Universidade Federal de Lavras (UFLA), 37200-000 Lavras, MG, Brazil
[d] Brazilian Center for Research in Energy and Materials (CNPEM), Brazilian Synchrotron Light Laboratory (LNLS), 13083-970 Campinas, SP, Brazil

ARTICLE INFO

Keywords:
Density functional theory
X-ray magnetic circular dichroism
Hybridization
Induced magnetic moments
Fe/Co alternated ultrathin films
Nonmagnetic/ferromagnetic interfaces

ABSTRACT

The induced magnetization in Cu atoms at the interface between ferromagnetic (FM) Fe/Co ultrathin films and a nonmagnetic (NM) Cu_3Au(001) substrate was explored by the investigation of two structures of five alternated Fe and Co monoatomic layers with different stacking orders with a Fe or a Co layer in direct contact with the Cu_3Au (001) surface. First principles calculations were applied to disentangle the origin of magnetic proximity effects at these FM/NM interfaces. The hybridization between the electronic states of the FM layers, resulting in a pronounced widening of the d-bands of the local density of states of Fe-Co interface atoms, has a fundamental effect in the spin-polarization of the NM substrate. X-ray magnetic circular dichroism measurements at the $L_{2,3}$-edges of Fe, Co and Cu allowed to extract the spin and orbital magnetic moments of Fe and Co, and to measure extremely low magnetic moments induced in Cu atoms. It is shown that the magnetism is induced only in the Cu and Au atoms at the first CuAu monolayer at the very surface of the substrate, i.e., the Cu XMCD signal is due to only 0.5 ML magnetic Cu atoms.

1. Introduction

The induced magnetism of nonmagnetic materials in proximity with ferromagnets has been extensively studied [1–9]. Ferromagnetic/nonmagnetic (FM/NM) heterostructures are very relevant to technological applications, as spintronic devices, sensing technologies and memory devices [10,11]. It has been shown, for instance, that induced magnetic moments can affect the spin Hall effect, spin transport and spin damping properties, and such effect can play an important role in technologies based on domain wall motion, as well as in spin torque memories [12–17]. A better understanding of induced magnetism at FM/NM heterostructures should lead to important improvements in these fields, and enrich the discussion on other related phenomena.

An induced magnetization has been theoretically predicted for Pd, Rh, and Pt in multilayered structures with Fe and Co [1,2,18,19]. These elements are close to satisfying the Stoner criterion to magnetism [20], and an induced magnetization should be anticipated. Furthermore, the spin polarization of these 5d elements, in the neighborhood of *3d* transition elements, has been experimentally demonstrated taking advantage of the element selectivity of X-ray magnetic circular dichroism (XMCD) [1,15,16,21–24] and other techniques [7,8,16,17]. XMCD technique is particularly suitable for the investigation of induced magnetism. It is element specific and has a high sensitivity that allows the measurements of extremely low magnetic signals [25]. The XMCD signal is an average over all atoms of each specie and it is not possible to separate the signal of different layers of the same element as is the case of X-ray resonant magnetic scattering (XRMS) [26,27]. Despite that, since magnetic induction is an interfacial phenomenon and XMCD is more sensitive to the surface, the averaging is restrict to only the interface and a few monolayers. Furthermore, it is possible to extract

* Corresponding authors.
E-mail addresses: zacarias@ifi.unicamp.br (E.Z. da Silva), wmacedo@cdtn.br (W.A.A. Macedo).
[1] Co-first authors.
[2] Present address: Instituto Madrileño de Estudios Avanzados en Nanociencia (IMDEA Nanoscience), E-28049 Madrid, Spain.

https://doi.org/10.1016/j.apsusc.2021.149215
Received 28 November 2020; Received in revised form 9 January 2021; Accepted 30 January 2021
Available online 5 February 2021

separately the spin and orbital magnetic moments of each element applying sum rules [25].

The hybridization of d-orbitals by the proximity effect at a NM/FM interface influences the electronic and magnetic properties of both materials, and the NM can become FM in thin films and multilayers where the density of states is enhanced by band narrowing [22–28]. It can lead to the induction of magnetism even in materials that have Stoner parameters far away from the unity required to fulfill Stoner criterion for a FM stability. It has been investigated, for example, how hybridization with Co gives rise to a magnetic moment in the interfacial atoms of the noble metals Cu, Ag and Au [29]. An induced magnetization has been observed in Cu atoms in layered systems like Fe/Cu, FeCu/Cu, Co/Cu, Gd/Cu or Co/Cu/Pt multilayers, and also in Cu nanoparticles embedded in Co [3–6,30,31]. There are also different studies on induced spin polarization in metallic Au atoms in Fe/Au multilayers [32–35], but no report on studies of spin polarization in FM/Cu-Au interfaces was found.

Cu and Cu-alloy substrates play an important role among the nonmagnetic surfaces often used for the epitaxial growth of *3d* FM ultrathin films. More specifically, ordered $Cu_3Au(001)$ has been used as a substrate to study the correlation between the structure and the magnetic properties of epitaxial FM *3d* metal and alloy films, mostly with focus on magneto-volume and structural effects [36–40], exchange bias [41,42], and tuning of the magnetic anisotropy [43,44].

The capability of tailoring the magnetic anisotropy of ultrathin films and layered nanostructures has been also a topic of particular scientific interest for a long time, since a large perpendicular magnetic anisotropy (PMA) is a key feature for spintronic devices [45]. It has been theoretically predicted that a tetragonal distortion of Fe-Co thin films can lead to a giant PMA for specific alloy compositions [46]. For Fe-Co, PMA and the influence of tetragonal distortion induced by epitaxial growth on NM substrates is an intensively investigated topic [43,46–50]. Besides the tetragonal distortion, chemical order has also been theoretically predicted to favor PMA in Fe-Co epitaxial ultrathin films [51]. Due to the interatomic distance of 2.64 Å, $Cu_3Au(001)$ has been suggested as a promising substrate for the growth of Fe-Co films with a large PMA [51]. We have previously studied the structural and magnetic properties of alternate Fe and Co monolayers epitaxially grown on $Cu_3Au(001)$ [43], a system that results in chemically ordered Fe/Co ultrathin films with a tetragonally distorted $L1_0$ structure [43,44]. In this system, the growth-induced ordering plays also an important role in the different contributions boosting PMA [51].

In view of the importance of epitaxial Fe-Co ultrathin films as magnetic nanostructures [46,47,51–54], and also of the magnetism induced by proximity effect at FM/NM interfaces [1–10], the Fe-Co/$Cu_3Au(001)$ is an interesting candidate for the investigation of induced magnetization. This system has a more complex electronic structure than the FM/Cu or FM/Au systems, due to the hybridization of the FM atoms with both Cu and Au interfacial atoms, which should affect the magnetic properties of the heterostructure.

In this work, we have investigated the induction of magnetism in Cu and Au atoms at the interface between ultrathin epitaxial films of alternate Fe/Co monolayers and a $Cu_3Au(001)$ substrate. The influence of the interface on the induced moment has been explored by growing Fe or Co as the very first magnetic monolayer in direct contact with the Cu_3Au surface, while the total thickness of each Fe/Co stack was maintained constant in 5 monolayers (ML). The precise mechanism of the hybridization at the FM/NM metal interface was investigated by density functional theory (DFT) calculations. The spin and orbital magnetic moments were experimentally determined by means of X-ray absorption spectroscopy (XAS) and X-ray magnetic circular dichroism (XMCD) measurements at Fe, Co, and Cu $L_{2,3}$-edges. Our results attest the induction of magnetic moments in the interfacial Cu atoms, as also clearly demonstrated the importance of the interface on the electronic and magnetic properties of nonmagnetic and ferromagnetic atoms.

2. Theoretical methods and computational approach

The epitaxial growth of alternate magnetic MLs of Fe and Co on the $Cu_3Au(001)$ substrate was simulated at atomistic level by *ab initio* density functional theory [55], using the spin-polarized generalized gradient approximation (GGA) [56] with exchange and correlation energy functional proposed by Perdew–Burke–Erzenhof (PBE) [57]. It provided a careful description of the formation of magnetic moments of the deposited magnetic MLs, as well as the induced magnetic moments in the nonmagnetic substrate. Charge and spin densities [58,59] were used to study many magnetic properties of this system. DFT-PBE investigations are well accepted as a computational framework, which is used in a wide range of DFT investigations and yields magnetic calculations similar to the hybrid exchange and correlation functionals with smaller computational cost [60]. The projector augmented-wave (PAW) method [61,62] was employed to computationally solve the Khon-Sham equations, as implemented in the Vienna *ab initio* Simulation Package (VASP) – version 5.4.4 [63,64]. The electron–ion interactions of the magnetic and nonmagnetic materials were described with the following PAW projectors: Au($5d^{10}6s^1$), Cu($3d^{10}4s^1$), Fe($3d^74s^1$), and Co($3d^84s^1$), where the valence states are shown in parenthesis.

To simulate the induced magnetic moments and the interface properties of the [Fe(Co)(001)]/$Cu_3Au(001)$ surface, we first converged the bulk structures of iron (Fe), cobalt (Co) and auricupride (Cu_3Au). The surfaces were calculated with the total forces cutoff of 466 eV, which is 12.5% larger than the cutoff energies recommended by the VASP package. In order to access the reliability of the effect of deposition of Fe and Co magnetic MLs on the $Cu_3Au(001)$ surface, we evaluated first the free Fe and Co MLs, the free Fe/Co double layer (DL), and the pristine $Cu_3Au(001)$ surface.

The equilibrium geometries were reached when all forces in the atoms were smaller than the 0.01 eVÅ^{-1} on every atom. The electronic convergence criterion for the self-consistent Kohn-Sham equations adopted in our calculations was 10^{-7} eV. Also, for the Brillouin zone integration, a k-mesh of 9×9×9 was used for the bulk geometries, while a 9×9×2 one was used for the surfaces, in the structural optimizations. However, to obtain a better description of the electronic properties, a k-mesh twice of the structural relaxations was employed to simulate the electronic properties such as density of states, and the charge investigations. In order to avoid the partial electronic occupations, the adopted width of the Gaussian smearing of 0.01 eV was employed. To avoid spurious interactions between the images in the periodic calculations, we used a minimum vacuum thickness of 15 Å in the growth direction. In order to compare the simulations with the experiments, we calculated the charge and the spin charge density difference ($\Delta\rho\uparrow\downarrow = \rho\uparrow - \rho\downarrow$) for each geometry.

We also employed the noncollinear investigations within the spin–orbit coupling (SOC) methodology, as implemented in the VASP package by Hobbs, Kresse, Marsmann and Hafner [65,66]. This technique allows to obtain a self-consistent calculation of the orbital magnetic moments for the deposited magnetic monolayers, which shows a moderate SOC, and for the unpolarized atoms.

These calculations were compared with the values derived from the application of sum rules to the XMCD measurements at the $L_{2,3}$ absorption edges of Fe, Co and Cu in the alternate Fe/Co MLs epitaxially grown on the $Cu_3Au(001)$ surface. The obtained results help to understand the magnetic properties at the Fe-Co/$Cu_3Au(001)$ interfaces i.e., the hybridization and spin polarization at these NM/FM interfaces, which is a challenging task.

3. Experimental methods

The samples were prepared in an ultra-high vacuum (UHV) chamber with a base pressure of 2×10^{-10} mbar. The $Cu_3Au(001)$ substrate was prepared by successive cycles of Ar^+ sputtering (1.5 keV) and annealing (670 K), repeated until a clean and well-ordered surface was observed. E-

beam evaporators were used to epitaxially grow stacks of alternate monoatomic layers (1 ML) of Fe and Co on the prepared $Cu_3Au(001)$ substrate. The Fe/Co films were grown at 300 K, with a constant evaporation rate around 0.5 ML/min, and using shutters to control the alternate Fe or Co deposition. The evaporation rate was calibrated using a quartz microbalance and RHEED oscillations. Two 5 ML thick epitaxial stacks were prepared, starting with the evaporation of 1 ML of Fe or Co, in order to obtain Fe/Co ultrathin films of the same total thickness, but with different interfaces, i.e., different magnetic monolayers, Fe or Co in direct contact with the $Cu_3Au(001)$ substrate: (i) $FeCoFeCoFe/Cu_3Au(001)$ (Stack A), and (ii) $CoFeCoFeCo/Cu_3Au(001)$ (Stack B). Low energy electron diffraction (LEED) and reflected high-energy electron diffraction (RHEED) were used to monitor the layer-by-layer growth and structure of the samples. After the growth of the alternate Fe/Co MLs ultrathin films, the samples were transferred from the preparation chamber to the experimental station in UHV conditions, with the use of a vacuum suitcase. The base pressure during transfer was always better than 10^{-9} mbar, and no oxidation on Fe and Co was observed after the transfer.

The element-specific magnetic properties of both samples were probed by XAS/XMCD experiments performed at the PGM beamline of the Brazilian Synchrotron Light Laboratory (LNLS) [67]. The absorption spectra for Fe, Co and Cu $L_{2,3}$-edges were acquired using the total electron yield mode, with the photon beam with right and left polarizations (80% circular polarization), at normal (0°, NI) and grazing (60°, GI) incidences, where the angle is defined between the surface normal and the X-ray propagation direction. The spectra were acquired with energy resolution of 0.2 eV, and measured at 300 K (for both samples) and also at 30 K (only for Stack B), with a magnetic field of 1.0 T applied parallel to the X-rays beam axis. From our previous experiments on similar films of alternate Fe/Co monolayers grown on $Cu_3Au(001)$ [43], we can clearly affirm that an applied field of 1.0 T is sufficient to saturate the film magnetization in both directions.

4. Results

4.1. Theoretical calculations

In order to develop a clear picture of the formation of magnetic moments in the deposited magnetic Fe and Co MLs on the $Cu_3Au(001)$ surface, the magnetic induction on the Cu and Au interface atoms, and the consequences of all these effects, we performed theoretical calculations to help the understanding of the observed experimental results.

We first calculated the magnetic structure of hypothetical free-standing Fe and Co MLs, and also a free standing Fe/Co double layer (DL) with the in-plane crystalline parameters of $Cu_3Au(001)$. Although these results are artificial, they help to set limits to the results of the deposited magnetic MLs on the $Cu_3Au(001)$ surface. The results of the magnetic moments of the free standing Fe and Co MLs are $m_S(Fe) = 3.09\ \mu_B$ and $m_S(Co) = 2.10\ \mu_B$, respectively. These results of high magnetic moments are due to two factors, the reduced geometry provided by the ML geometry as well as the large lattice spacing imposed by the $Cu_3Au(001)$ surface lattice parameter. Of course, these are upper bounds for the results of the real alternated Fe and Co MLs deposited on the $Cu_3Au(001)$ surface. The double layer (DL) also provides some insights as upper bounds. The calculated magnetic moments for the free FeCo DL are $m_S(Fe) = 2.75\ \mu_B$ and $m_S(Co) = 1.66\ \mu_B$. The magnetic moments for the DL are reduced due to the interlayer interaction between Fe and Co layers. The DL structure allows the overlap of Fe and Co wave functions, which lowers the magnetic moments and widens their *d* bandwidths. All these calculations were performed for the $Cu_3Au(001)$ surface lattice spacing that in the real system provides the template in which the stacks of alternate Fe and Co MLs were grown (the density of states (DOS) of the free-standing metal MLs and DL are shown in the SM, Fig. S1).

We also calculated the pristine $Cu_3Au(001)$ surface. This ordered fcc [001] structure can be viewed as the stacking sequence of alternating Cu-Cu and Au-Cu MLs. Fig. 1(a) shows the slab used to simulate this surface. The electronic structure of the $Cu_3Au(001)$ surface, and also of the two epitaxial FM/NM stacks focus of the present study (Stack A and Stack B) were calculated and compared with the experiments. All the structures are presented in Fig. 1.

The effect of the magnetic Fe and Co MLs on $Cu_3Au(001)$ can be observed in Fig. 2, that depicts the DOS of the *d*-Cu and *d*-Au states in top layer (TL) atoms, where we compare the effect of the magnetic MLs on the Cu and Au atoms at the very FM/NM interface. In Fig. 2, it is important to observe that there is a shift towards lower energies in the Cu and Au atoms, due to the effect of the magnetic MLs. The deposition of the magnetic MLs lowers the energies of the Cu and Au occupied states. The Au DOS was already at lower energies compared to the Cu DOS for the pristine surface. It lowered a little more upon interaction with the magnetic MLs and, as a consequence, TL Au hybridization with magnetic MLs is less effective. For this reason, the magnetic induction is more effective on the TL Cu atoms.

The monolayer-resolved Fe and Co DOS for the alternate Fe/Co monolayer structures, with Fe (Stack A) or with Co (Stack B) at the $Cu_3Au(001)$ interface, depicted in Fig. 3, show the evolution of the magnetic moments associated with the electronic states (see Table S1 in the SM).

Many aspects of the magnetism of these deposited FM MLs can be understood with the analysis of their electronic states. It can be seen in the Fig. S1 that a free Fe or Co ML has a narrow DOS, in the range of the Cu states at the TL. Therefore, the hybridization with this surface is not as effective. The free-DL DOS, however, widens considerably due to the hybridization between the wave functions of each ML. In this manner, when more than one ferromagnetic ML is deposited on the $Cu_3Au(001)$ surface, induction and interaction between the FM film and the NM surface are more effective, causing the widening of the DOS in the energy region of the *d*-Fe and *d*-Co states. Also, the first deposited magnetic ML hybridizes with the $Cu_3Au(001)$ surface, lowering its magnetic moment, when compared with the free magnetic ML. If there was just this ML, it would still have a free surface, and the magnetic moments would be still high, but with a value smaller than for the free-standing ML, being less effective towards inducing magnetism in Cu and Au surface (TL) atoms. However, in the present case there is another magnetic ML on top of the interfacial magnetic ML, which by itself already broadens their DOS. In this situation, the double layer interfaced with

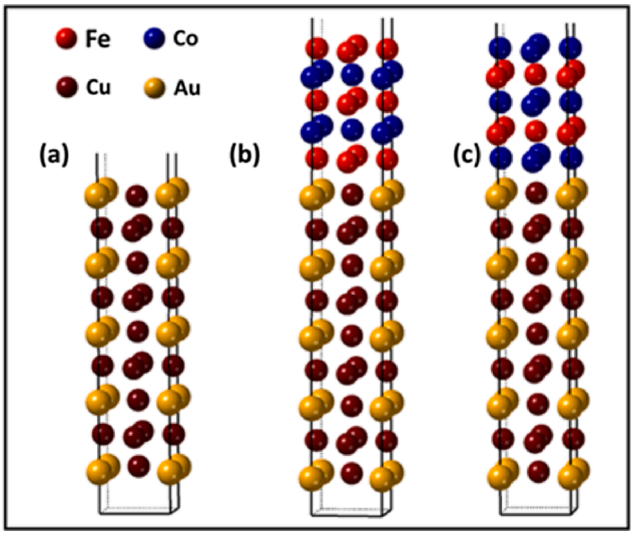

Fig. 1. Structures used in the DFT calculations: (a) $Cu_3Au(001)$ surface, (b) Stack A, and (c) Stack B. The atoms in the structures are depicted in colors: Au (yellow), Cu (brown), Fe (red), and Co (blue). (For interpretation of the references to color in this figure legend, the reader is referred to the web version of this article.)

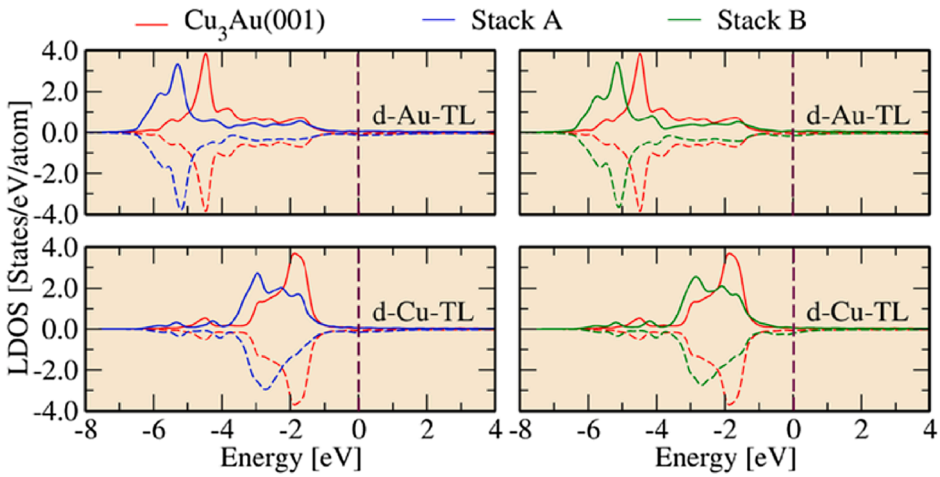

Fig. 2. Local density of states (LDOS) per atom. In the top panels are shown the *d*-Au-TL and, in the bottom panels, the *d*-Cu-TL electronic contributions, without (red lines) and with the deposited magnetic material depicted in Stack A (blue lines) and Stack B (green lines). (For interpretation of the references to color in this figure legend, the reader is referred to the web version of this article.)

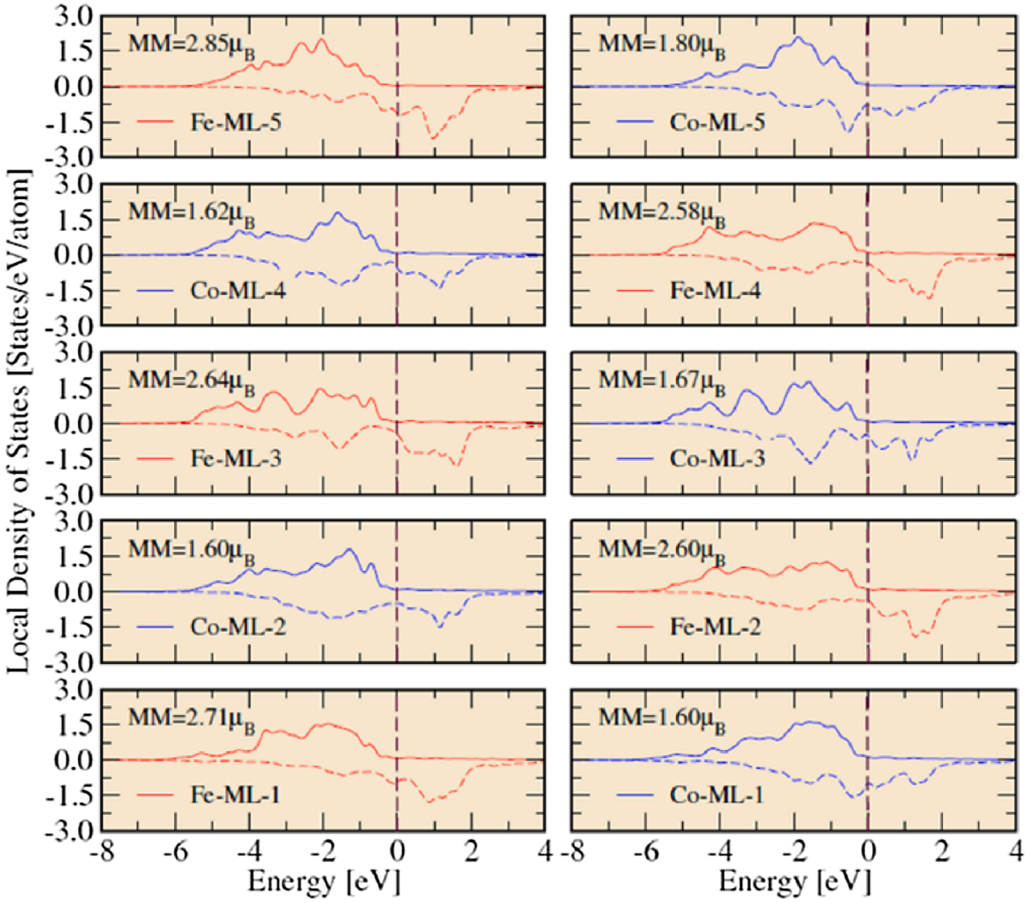

Fig. 3. Layer-resolved Fe and Co local density of states (LDOS) for the 5 MLs Fe/Co on $Cu_3Au(001)$ samples (Stack A, in the left, and Stack B, in the right), in the stacking sequence order. The obtained localized magnetic moment (MM) is shown for each magnetic ML.

the $Cu_3Au(001)$ surface is more effective in inducing magnetic moments on Cu and Au surface atoms. Therefore, both structures, with Fe and with Co at the interface, start with magnetic MLs with a small reduction of their magnetic moment, when compared to the free double layer, but are more effective in the hybridization effect. All the other internal magnetic MLs are sandwiched by the other species, and their magnetic moments stay almost constant at intermediate values, which is a consequence of the interlayer interaction. Finally, in the top magnetic ML, with a free surface, the hybridization results in a narrowing in the DOS and an enhancement in its magnetic moment. In fact, their magnetic moment is higher than the values of the free DL.

All these results end up giving average spin magnetic moments for each atom species with values of $m_S(Fe) = 2.73\ \mu_B$ and $m_S(Co) = 1.61\ \mu_B$ for Stack A; and $m_S(Fe) = 2.58\ \mu_B$ and $m_S(Co) = 1.69\ \mu_B$ for Stack B, as

listed in Table 1 and Fig. S2. The numbers of *3d* empty states for the different elements, obtained from the DOS calculations, are listed in the SM, Table S2. Therefore, an aspect emerges from the calculations: a geometric effect is at play for this odd number of layered structures. In Stack A, the interfacial magnetic ML, being the first ML attached to a nonmagnetic interface, and the top ML, which has a free surface, have their magnetic moments enhanced when compared to the internal layers, in contrast with the Stack B. This is due to a small lowering of the magnetic moment at the nonmagnetic interface, and to the enhancement of the magnetic moment on the surface top layer.

The induced spin magnetic moments on the Cu and Au interfacial atoms are higher in the case of Stack A than in the case of Stack B. Moreover, the induction is always higher for Cu atoms than for Au atoms, regardless of the FM interface. As discussed before, the hybridization of the deposited magnetic MLs is more effective with the Cu atoms, resulting in higher spin moments. The Au surface atoms have their more important states at lower energies, as compared with the Cu ones. On the other hand, the orbital magnetic moments induced on Au atoms are one order of magnitude larger than those induced on Cu atoms (see Table S1). This behavior is due to the fact that the atomic radius of Au is greater than the Cu, which provides large angular moments for Au compared to Cu atoms.

4.2. Experimental characterization

The epitaxial growth and structural characterization of the alternate Fe/Co atomic monolayers on the $Cu_3Au(001)$ substrate has been already described in a recent work [43] for Fe at the interface (Stack A), in which it is shown that the alternated deposition leads to an almost layer-by-layer growth up to 6 ML. Moreover, magneto-optical Kerr effect (MOKE) measurements for films of alternate Fe/Co monolayers and codeposited FeCo films clearly demonstrate the effect of the chemical ordering in the magnetic properties of the system [43]. For Co at the interface (Stack B), some complementary LEED and RHEED data are presented in Fig. S5 of the SM. Absorption spectra were acquired at Fe, Co and Cu $L_{2,3}$-edge at magnetic fields of 1.0 T at normal (0°) and grazing (60°) incidences and temperatures of 300 K (both stacks) and 30 K (only Stack B). All spectra were normalized at the maximum of the L_3-edges of isotropic XAS, which is defined as the average of absorption spectra with positive and negative circular polarizations. XMCD is the difference between both polarizations.

Fig. 4 presents the room temperature (300 K) XAS/XMCD spectra measured for the Stack A. The shapes of all XAS spectra are characteristic of metallic materials, and no indication of sample oxidation is observed. One should notice that such measurements are particularly sensitive to the surface, and the presence of any oxide would appear as shoulders or peaks at the high energy side of the L_3 peaks. As can be seen in Fig. 4(c) and (f), there is a clear induced magnetism in Cu atoms. For a better visualization, Cu XMCD spectra are shown multiplied by a factor of 20. In spite of the low signal to noise ratio, a Cu dichroic signal can be observed at both incidences. The XMCD intensities of Fe and Co are very similar when comparing the two incidences, which confirms that the Fe/Co film is saturated. In the case of Cu, the high noise level hinders a qualitative comparison of the spectra for the different incidences.

Normalized $L_{2,3}$ XAS and XMCD spectra for Stack B, measured at 300 K, are presented in Fig. 5, and also have metallic shapes. The Cu spectra were averaged from a higher number of measurements, in order to increase the signal/noise ratio. With this procedure, the shape of the averaged spectra were better defined when compared with Stack A, as can be observed in Fig. 5(c) and (f). In this case, it was possible to compare the two Cu spectra, and there is no significant difference between the XMCD signals for both incidences, as observed for Fe and Co.

For this Fe/Co sample (Stack B), additional measurements have been done also at low temperature (30 K), and these spectra are shown in Fig. 6. When comparing Fig. 5 (300 K spectra) and Fig. 6 (30 K spectra), it is possible to observe an increase of the XMCD signal at the Fe and Co edges at low temperature. For the Cu $L_{2,3}$-edge, there is no evident change in the XMCD signal with the temperature.

The magnetic moments of the Fe, Co and Cu atoms in both samples have been extracted from the XMCD data shown in Figs. 4–6 by applying sum rules [68,69], and corrected for the 80% degree of polarization of the X-rays at the beamline. The numbers of *3d* empty states used in the sum rules calculations were those determined theoretically by our DFT calculations for each structure and presented in Table S2, in the SM. The number of Fe and Co empty states is given by the average of all Fe or Co layers in each case. For Cu, the number of 3*d* empty states refers only to the atoms at the surface layer of the $Cu_3Au(001)$, since our DFT results indicate that a significant magnetic moment is induced only at the first interfacial layer of the NM substrate (see Fig. S4, in the SM). This behavior is similar to the observed for the magnetic moment induced by Co atoms in a Rh substrate [24,70], for example.

From the sum rules it is possible to extract the values of the orbital moment (m_L) and the effective spin moment (m_{eff}). The m_{eff} is a sum of two components: the spin magnetic moment (m_S) and the dipolar magnetic term (7D), i.e., $m_{eff} = m_S + 7D$. Although the dipole term is negligible for bulk 3*d* metals, in the case of ultrathin films, due to the low symmetry, this term is significant and has to be considered to allow an accurate determination of the spin moment. For a system with uniaxial anisotropy it is possible to separate these two components by angle-dependent XAS/XMCD measurements [71–73]. At saturation, the m_S is independent of the angle, and the dipolar term at an angle θ was shown to be [73,74]: $7D(\theta) = \frac{7D(0^\circ)}{2}(3cos^2\theta - 1)$. Considering this relation and the values of m_{eff} extracted by sum rules from the spectra acquired at normal (0°) and grazing (θ = 60°) incidences, it was possible to estimate the dipole term, 7D(0°). All these experimental values are presented in Table S3 of the supplementary material.

Having in mind that the Cu XMCD signal carries a significant contribution from unpolarized Cu atoms of the $Cu_3Au(001)$ substrate, the obtained values need to be corrected in order to allow a reasonable estimation of the induced magnetization in the Cu interface atoms, since, as shown by the calculations (see Fig. S4 in SM), only those atoms present a significant magnetism. Assuming an electron mean free escape depth of ~20 Å (11 ML) [5], and taking into account the different angles of incidence of the photon beam, we obtain multiplicative correction factors of 9.1 and 4.5 for the measurements at normal (0°) and grazing (60°) incidences, respectively.

Table 1
DFT results for Fe, Co, Cu and Au atoms in the two epitaxial stacks of alternate Fe/Co monoatomic layers on $Cu_3Au(001)$. The indicated spin magnetic moment ($\mathbf{m_S}$) and orbital magnetic moment ($\mathbf{m_L}$) values are the averages for all atomic sites of each element in the sample, at 0 K. Layer-resolved values can be found in Table S1 of the supplementary material.

		Stack A (Fe interface)	Stack B (Co interface)
Fe	$\mathbf{m_S}$	2.73	2.58
	$\mathbf{m_L}$	0.07	0.06
Co	$\mathbf{m_S}$	1.61	1.69
	$\mathbf{m_L}$	0.07	0.09
Cu	$\mathbf{m_S}$	0.044	0.020
	$\mathbf{m_L}$	0.001	−0.002
Au	$\mathbf{m_S}$	0.030	0.015
	$\mathbf{m_L}$	0.020	0.015

5. Discussion

Initially we compare our theoretical and experimental results. We recall that besides being element sensitive, XMCD is also orbital selective. In our case, measurements at $L_{2,3}$ absorption edges of *3d* elements probe mostly the *3d* levels of them. Thus we must compare the moments obtained from the application of sum rules on the XMCD data with the *3d* magnetic moments arising from the DFT calculations. Table 2 lists the

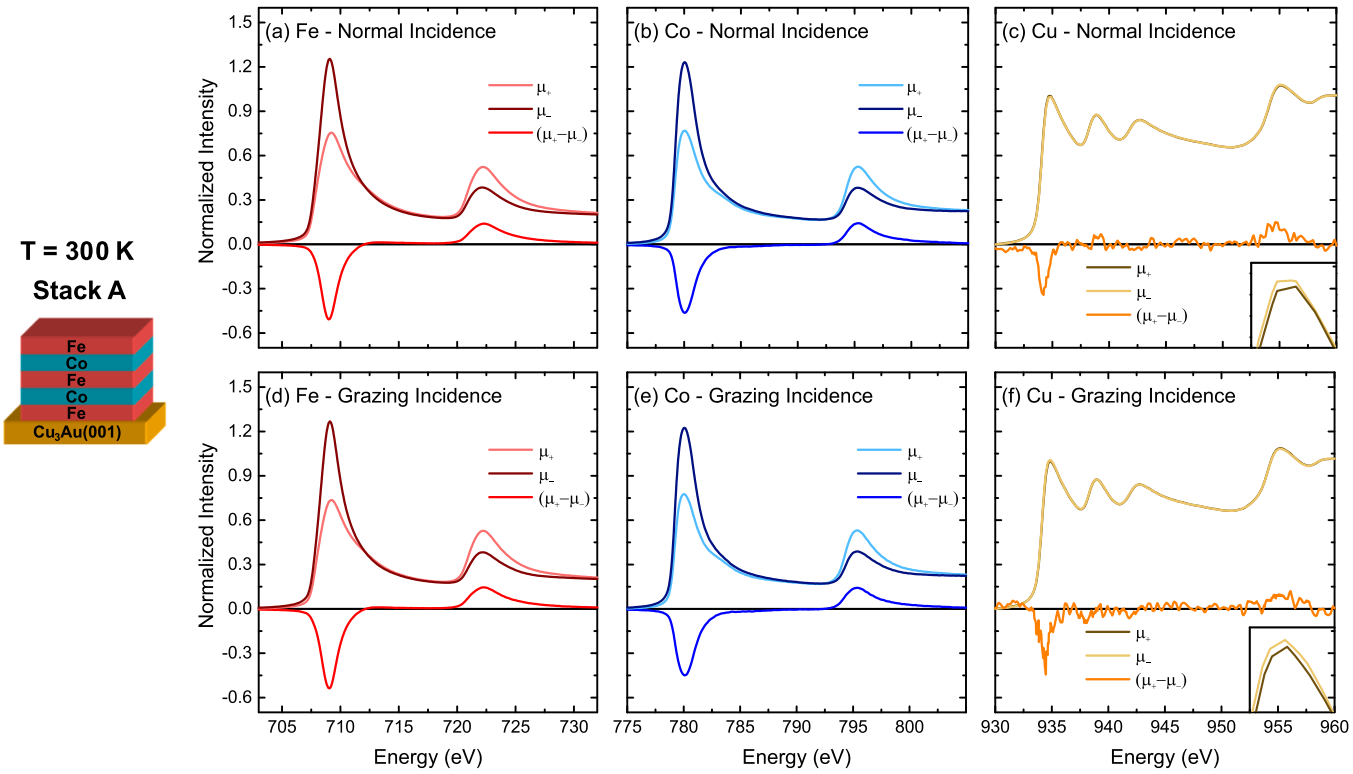

Fig. 4. Normalized X-rays absorption curves (μ+ and μ−) and XMCD spectra taken at normal (a-c) and grazing (d–f) incidences for the Fe (a,d), Co (b,e), and Cu (c,f) $L_{2,3}$-edges in the Stack A (schematic representation in the sketch), at room temperature (T = 300 K, B = 1.0 T). A zoom in the L_3 peak of Cu is displayed in the inset in (c) and (f), to allow a better visualization of the difference between the two absorption curves.

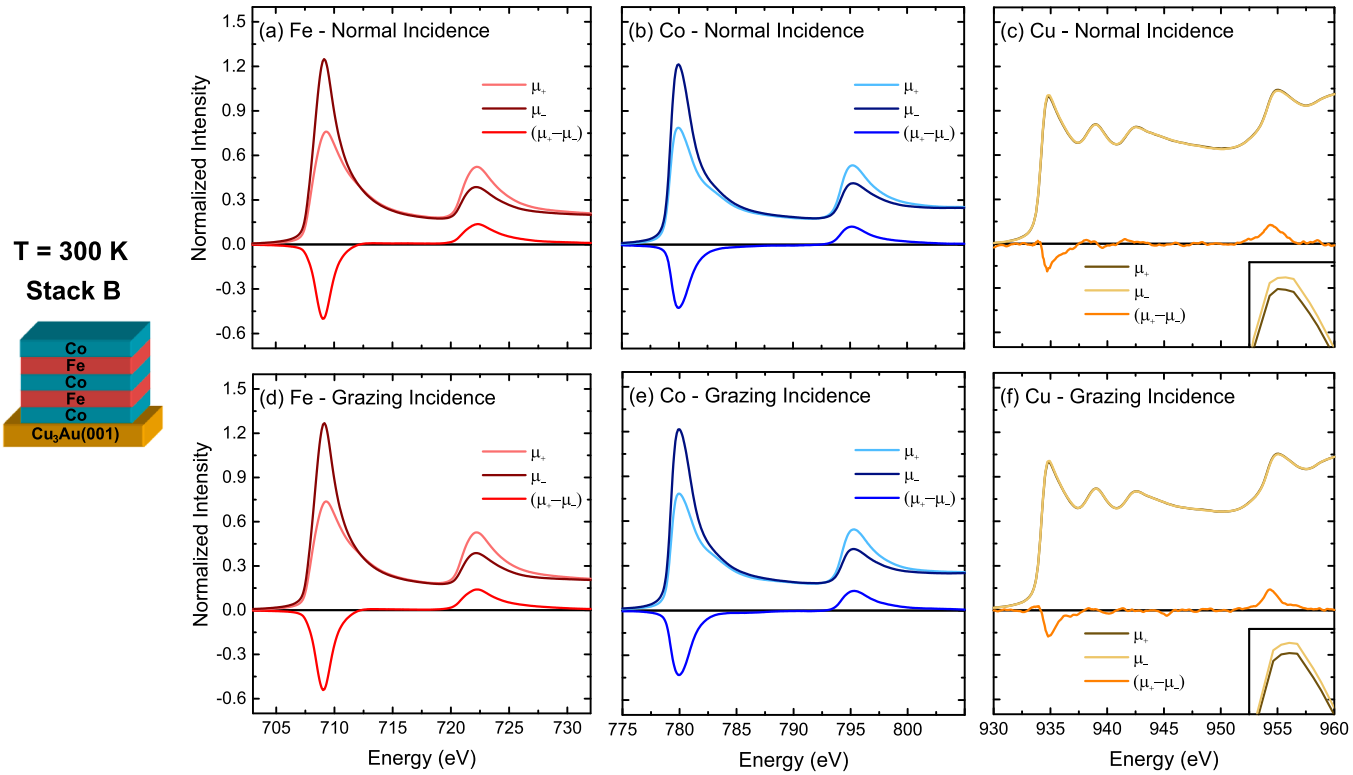

Fig. 5. Normalized X-rays absorption curves (μ+ and μ−) and XMCD spectra taken at normal (a–c) and grazing (d–f) incidences for the Fe (a,d), Co (b,e), and Cu (c,f) $L_{2,3}$-edges in the Stack B (schematic representation in the sketch), at room temperature (T = 300 K, B = 1.0 T). A zoom in the L_3 peak of Cu is displayed in the inset in (c) and (f), to allow a better visualization of the difference between the two absorption curves.

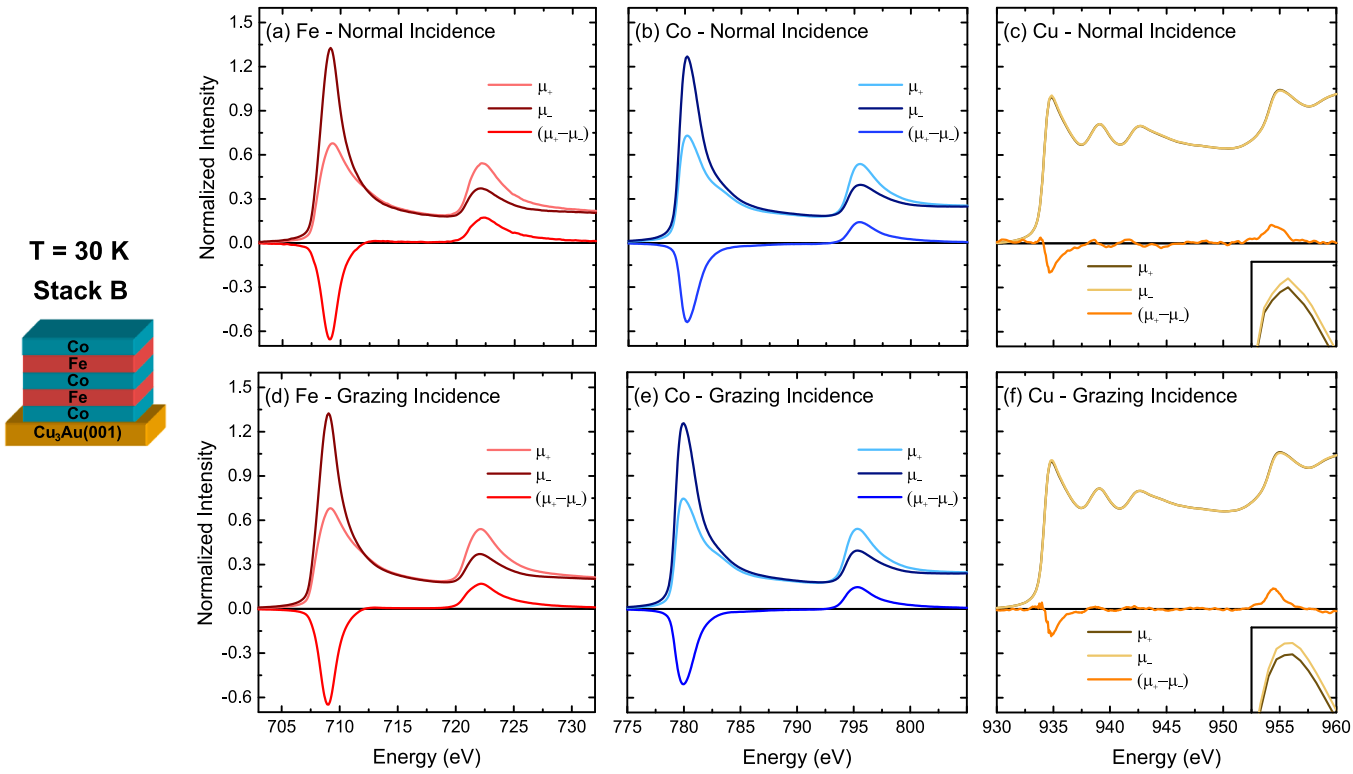

Fig. 6. Normalized X-rays absorption curves (μ+ and μ−) and XMCD spectra taken at normal (a-c) and grazing (d–f) incidences for the Fe (a,d), Co (b,e), and Cu (c,f) $L_{2,3}$-edges in the Stack B (schematic representation in the sketch), at room temperature (T = 30 K, B = 1.0 T). A zoom in the L_3 peak of Cu is displayed in the inset in (c) and (f), to allow a better visualization of the difference between the two absorption curves.

experimental XMCD results for the *3d* spin magnetic moments, obtained after the subtraction of the dipole term, and the values of the orbital magnetic moments for normal and grazing incidences. Note that for Cu are listed the values corrected to exclude the substrate contribution (Cu*), as above mentioned. This table includes also the *3d* magnetic moments determined theoretically by the DFT calculations. The theoretical Fe and Co magnetic moments are the average of the values of the 2 or 3 Fe and Co monolayers present in each structure. For the sake of direct comparison with the XMCD results, the DFT values quoted in Table 2 are those directly associated with the *3d* levels. One can notice that in Table 2 the values are larger than the total moment calculated by DFT (see Table 1). This arises from the fact that the *4s4p* orbitals have a negative contribution, and thus, the total moments end up smaller than the *3d* moments. For Fe and Co, this difference is of the order of a few percent, but it turns out to be not negligible for Cu, where 3*d* moments are of the same order of magnitude of the *4s4p* contribution.

Table 2
3*d* spin magnetic moment ($\mathbf{m_S}$) and orbital magnetic moment ($\mathbf{m_L}$) for Fe, Co and Cu atoms, in μ_B, calculated theoretically, and determined experimentally by XMCD sum rules, for the Stack A and Stack B for temperatures (Temp) of 0, 30 and 300 K.

		Stack A		Stack B		
		Experiment	Theory	Experiment		Theory
Temp.		300 K	0 K	300 K	30 K	0 K
Fe	m_S	2.11(21)	2.75	2.05(22)	2.43(27)	2.63
	$m_L(0°)$	0.15(1)	0.07	0.19(2)	0.25(2)	0.06
	$m_L(60°)$	0.21(2)	0.07[#]	0.23(2)	0.27(3)	0.05[#]
Co	m_S	1.50(16)	1.69	1.47(15)	1.70(17)	1.73
	$m_L(0°)$	0.25(3)	0.07	0.27(3)	0.34(3)	0.09
	$m_L(60°)$	0.24(2)	0.07[#]	0.27(3)	0.32(3)	0.09[#]
Cu	m_S	0.023(6)	0.072	0.022(6)	0.020(6)	0.037
[*]	$m_L(0°)$	0.001(1)	0.001	−0.001 (1)	−0.002 (1)	−0.002
	$m_L(60°)$	0.001(1)	0.003[#]	−0.001 (1)	−0.001 (1)	0.002[#]

[*] Corrected experimental values, to exclude the substrate contribution (see text).
[#] In-plane theoretical values ($m_L(90°)$).

Considering first Stack A (Fe interface), the experimental spin magnetic moments (m_S) of Fe and Co are smaller than the theoretical ones, as can be observed in Table 2. It is important to point out that the effect of temperature is not considered in the theoretical calculations (the calculated magnetic moments are values at 0 K). Since Stack A was measured only at room temperature (300 K), the smaller experimental m_S values obtained from the XMCD measurements could be a consequence of thermal disorder of the spins in this ultrathin (5 ML thick) magnetic nanostructure. This effect will be discussed later for Stack B, with the comparison of the measurements at 300 and 30 K.

Contrariwise, the Fe and Co experimental orbital magnetic moments (m_L) are higher than the respective theoretical values. A similar divergence between theory and experiment was reported for Fe and Co films grown on Rh(111) and Pt(111) [24], where the same computational approach has been used. This may indicate that this theoretical approach does not reproduce well the orbital moments, despite of being effective in the determination of the spin magnetic moments.

We were also able to experimentally confirm the existence of an induced magnetic moment in the Cu atoms at the Fe-Co/Cu_3Au(001) interface. The experimental values of the induced spin moments are smaller than the theoretical ones. However, in this case, the small values together with the high intrinsic error of sum rules prevent a quantitative comparison between theory and experiment. The induced magnetism in the NM atoms is an interfacial effect, and, for this system, our results show that a significant moment is induced only at the first layer of the substrate (see Fig. S4). Also, it has been demonstrated experimentally and theoretically that in an ordered Cu_3Au(001) single crystal the very surface shows a gold enrichment, to a composition around $Au_{60}Cu_{40}$ [75]. This means that in our XMCD experiments we are measuring the

magnetism induced in only at ~0.4–0.5 ML of Cu atoms. These induced magnetic moments are extremely low and, therefore, very hard to be experimentally probed.

In spite of the quantitative divergences between the theoretical and experimental values obtained for the induced moments in the Cu atoms, there is a qualitative agreement on the nature of the magnetic induction at the NM interface. In both cases, m_S and m_L of the spin-polarized Cu atoms at the surface of the $Cu_3Au(001)$ substrate are observed to be ferromagnetically aligned with the Fe/Co film.

For the stack with Co at the interface (B), m_S and m_L have been experimentally determined for 300 K and 30 K measurements, as already mentioned. The obtained magnetic moments for Fe, Co, and Cu* atoms are given in Table 2. At the lower temperature (30 K), the experimental m_S of Fe and Co are very close to the theoretical values, confirming the effectiveness of the DFT calculations in reproducing the spin moments. For the XMCD measurements at 300 K, there is a significant decrease of these moments, evidencing the effect of thermal disorder in the magnetism of the ultrathin Fe/Co samples. These findings corroborate the previous affirmation that, for Stack A, the temperature plays a major role to the discrepancy of calculation with the experiment results.

For the Cu atoms in Stack B, the m_S values extracted from the 30 and 300 K measurements are almost the same, being even slightly higher at 300 K. This may be attributed to the low intensity of the Cu XMCD signal, near the experimental limit of detection, together with the high intrinsic error of the sum rules [76]. Nevertheless, given the very low XMCD intensity, and the lack of intermediary temperature measurements, more investigation is needed to determine unequivocally if the temperature has any effect on the induced magnetic moments. As observed for Stack A, there is a qualitative agreement between theory and experiments even with some divergences in the quantitative values. For Stack B, there is a ferromagnetic coupling in the case of the spin magnetic moments, while for the induced orbital magnetic moments is observed an antiferromagnetic coupling in both, theory and experiment (negative values in Table 2). This is one more evidence of the reliability of our results and the good agreement between the theoretical calculations and the experimental results.

Although XAS measurements at Au-edges were not possible at the LNLS PGM beamline, and an induction of magnetism in Au atoms could not be probed in our experiments, the theoretical calculations indicate that the spin magnetic moment induced in the Au atoms at the Cu_3Au (001) surface is smaller, when compared to the magnetization induced in Cu atoms, but that the orbital magnetic moment induced on Au atoms are much larger then in Cu atoms (see Table S2). Even if it was not possible to perform experiments for Au atoms due to experimental limitation of the beamline, a XMCD signal is also expected for Au, and could, in principle, be addressed in a hard X-rays beam line covering the Au $L_{2,3}$ absorption edges.

Induced magnetic moments have been observed previously in Cu atoms in systems like Fe/Cu, FeCu/Cu, Co/Cu, Gd/Cu or Co/Cu/Pt multilayers and nanoparticles [3–6,29–31]. Due to the interfacial nature of the proximity effect, in all these studies the intensity of the induced moments in NM atoms is dependent on the surface area in contact with the FM. In this way, for a Cu film sandwiched between two FM layers, the average induced moments in Cu atoms will decrease with the film thickness, since the internal layers will not be polarized as much as the interface atoms. While for Cu atoms in a 4 ML thick film in Co/Cu/Co trilayers an induced m_S (m_L) of 0.047 μ_B (0.001 μ_B) was found [3,4], for a thicker Cu film (50 Å, ~28 ML) the average Cu m_S (m_L) can drop to 0.005 μ_B (0.0003 μ_B) [31]. In addition, the intensity of the induced moments depends also, of course, on the strength of the magnetic moments of the neighbor FM material. For 13 ML thick Cu spacers between Co layers, the induced m_S (m_L) in Cu atoms is 0.014 μ_B (0.0001 μ_B), but between Fe layers these moments are clearly larger ($m_S = 0.022$ μ_B; $m_L = 0.0007$ μ_B) [3,4]. Anyway, the determination of subtle differences of spin polarization in Cu atoms at FM/NM interfaces like Fe/Cu and Co/Cu systems are expected to be experimentally very challenging, as shown in [4]. Moreover, for Cu atoms, the induced spin and orbital moments can be extremely small, making unfeasible the estimation by sum rules, as in XMCD measurements in Gd/Cu multilayers [30]. From our results, it turns out that the induced magnetization estimated for the Cu atoms at the very surface of the NM $Cu_3Au(001)$ in Stacks A and B ($m_S \sim 0.02$ μ_B; $m_L(A) \sim 0.001$ μ_B; $m_L(B) \sim -0.002$ μ_B) are of the same order of magnitude of those obtained in references [3,4,6,29], but are clearly much smaller than the induced magnetization in Cu atoms observed by Kuch et al. in artificially ordered FeCu superlattices where all the Cu atoms are expected to be in direct contact with Fe atoms, between Fe single layers [5]. In spite of the very small XMCD magnetic signal from Cu atoms in the nanostructures investigated in this work, consisting of alternate Fe/Co monoatomic layers epitaxially grown on $Cu_3Au(001)$, we have unequivocally probed the existence and estimated the magnitude of the induced magnetism in these NM atoms at the surface of the Cu-Au substrate.

6. Conclusions

In summary, using $L_{2,3}$-edges XAS/XMCD measurements, we have observed clear evidence of induced magnetic moments in Cu atoms, due to the proximity effect, in alternate Fe/Co monoatomic layers epitaxially grown on top of an ordered $Cu_3Au(001)$ single crystal. This is a remarkable result, considering the extremely low magnetic moments that are induced in the Cu atoms. The experimental results were compared with density functional theoretical calculations. The theoretical spin moments are in good agreement with the values derived from the experimental results, by the application of sum rules. Our results show that in the investigated system the magnetism induced in the nonmagnetic Cu (and Au) atoms is a phenomenon restrict essentially to the very interface. According to our theoretical calculations, the induction is more effective due to the hybridization from the first two magnetic layers, where the proximity between the magnetic and NM MLs is a relevant factor. Also, this hybridization with the NM Cu_3Au surface decreases the magnetic moments of the deposited Fe-Co atoms, in comparison to the Fe and Co free MLs and Fe/Co DL. The theoretical calculations reveal also the effect of the nonmagnetic surface and the vacuum interface in the enhancement of the magnetic moments of Fe and Co, and the effect of the hybridization at the interface on the magnetization profile of the remaining FM layers. Our experimental and theoretical results represent a contribution to the precise understanding of the induced magnetism at FM/NM interfaces.

CRediT authorship contribution statement

Sofia O. Parreiras: Investigation, Formal analysis, Writing - original draft. **Luis A. Cabral:** Investigation, Formal analysis, Writing - original draft. **Rodrigo V. Lourenço:** Investigation, Formal analysis, Writing - review & editing. **Alexandre A.C. Cotta:** Investigation, Writing - review & editing. **Pedro Schio:** Investigation, Writing - review & editing. **Julio C. Cezar:** Investigation, Writing - review & editing. **Pedro L. Gastelois:** Investigation, Writing - review & editing. **Edison Z. Silva:** Supervision, Writing - review & editing, Funding acquisition. **Waldemar A.A. Macedo:** Supervision, Writing - review & editing, Funding acquisition.

Declaration of Competing Interest

The authors declare that they have no known competing financial interests or personal relationships that could have appeared to influence the work reported in this paper.

Acknowledgements

The authors acknowledge financial support from the Brazilian Agencies Conselho Nacional de Desenvolvimento Científico e Tecnológico - CNPq (Grants 308321/2014-6 and 426937/2016-3, WAAM;

422583/2018-9, AACC; Fellowship 160595/2017-7, SOP), Fundação de Amparo à Pesquisa do Estado de Minas Gerais - FAPEMIG (Grant PPM-00431-17, WAAM), and Fundação de Amparo à Pesquisa do Estado de São Paulo - FAPESP (Grants 2018/20729-9, LAC; 2017/26105-4, 2016/23891-6 and 2013/07296-2, EZS). The theoretical investigations used the resources of the SDumont - Sistema de Computação Santos Dumont, and CCJDR-Unicamp - "Centro de Computação John David Rogers". The Brazilian Synchrotron Light Laboratory (LNLS/CNPEM) is acknowledged for beamtimes at the PGM beamline (Proposals 20170396 and 20180744, WAAM).

Appendix A. Supplementary material

Supplementary data to this article can be found online at https://doi.org/10.1016/j.apsusc.2021.149215.

References

[1] G. Schütz, S. Stähler, M. Knülle, P. Fischer, S. Parkin, H. Ebert, Distribution of magnetic moments in Co/ Pt and Co/Pt/Ir/Pt multilayers detected by magnetic x-ray absorption, J. Appl. Phys. 73 (1993) 6430–6432.
[2] E.E. Fullerton, D. StoefBer, K. Ounadjela, B. Heinrich, Z. Celinski, J.A.C. Bland, Structure and magnetism of epitaxially strained Pd(001) films on Fe(001): Experiment and theory, Phys. Rev. B 51 (10) (1995) 6364–6378.
[3] M.G. Samant, J. Stohr, S.S.P. Parkin, G.A. Held, B.D. Hermsmeier, F. Herman, Induced spin polarization in Cu spacer layers in Co/Cu multilayers, Phys. Rev. Lett. 72 (1994) 1112–1115.
[4] G.A. Held, M.G. Samant, J. Stöhr, S.S.P. Parkin, B.D. Hermsmeier, M. van Schilfgaarde, R. Nakajima, X-ray magnetic circular dichroism study of the induced spin polarization of Cu in Co/Cu and Fe/Cu multilayers, Z. Phys. B 001 (1996) 335–341.
[5] W. Kuch, M. Salvietti, M.T.Lin. Xingyu Gao, M. Klaua, J. Barthel, Ch.V. Mohan, J. Kirschner, Artificially ordered FeCu alloy superlattices on Cu(001). II. Spin-resolved electronic properties and magnetic dichroism, Phys. Rev. B 58 (13) (1998) 8556–8565.
[6] J. Okabayashi, T. Koyama, M. Suzuki, M. Tsujikawa, M. Shirai, D. Chiba, Induced perpendicular magnetization in a Cu layer inserted between Co and Pt layers revealed by x-ray magnetic circular dichroism, Sci. Rep. 7 (2017) 46132.
[7] R.M. Rowan-Robinson, A.A. Stashkevich, Y. Roussigné, M. Belmeguenai, S.-M. Chérif, A. Thiaville, T.P.A. Hase, A.T. Hindmarch, D. Atkinson, The interfacial nature of proximity induced magnetism and the Dzyaloshinskii-Moriya interaction at the Pt/Co interface, Sci. Rep. 7 (2017) 16835.
[8] O. Inyang, L. Bouchenoire, B. Nicholson, M. Tokaç, R.M. Rowan-Robinson, C. J. Kinane, A.T. Hindmarch, Threshold interface magnetization required to induce magnetic proximity effect, Phys. Rev. B 100 (2019), 174418.
[9] S. Mayr, J. Ye, J. Stahn, B. Knoblich, O. Klein, D.A. Gilbert, M. Albrecht, A. Paul, P. Böni, W. Kreuzpaintner, Indications for Dzyaloshinskii-Moriya interaction at the Pd/Fe interface studied by in situ polarized neutron reflectometry, Phys. Rev. B 101 (2020), 024404.
[10] F. Hellman, A. Hoffmann, Y. Tserkovnyak, G.S.D. Beach, E.E. Fullerton, C. Leighton, A.H. MacDonald, D.C. Ralph, D.A. Arena, H.A. Dürr, P. Fischer, J. Grollier, J.P. Heremans, T. Jungwirth, A.V. Kimel, B. Koopmans, I.N. Krivorotov, S.J. May, A.K. Petford-Long, J.M. Rondinelli, N. Samarth, I.K. Schuller, A.N. Slavin, M.D. Stiles, O. Tchernyshyov, A. Thiaville, B.L. Zink, Interface-induced phenomena in magnetism, Rev. Mod. Phys. 89 (2017), 025006.
[11] A. Hoffmann, S.D. Bader, Opportunities at the frontiers of spintronics, Phys. Rev. Appl. 4 (2015), 047001.
[12] K.S. Ryu, L. Thomas, S.H. Yang, S. Parkin, Chiral spin torque at magnetic domain walls, Nat. Nanotechnol. 8 (2013) 527.
[13] K.S. Ryu, S.H. Yang, L. Thomas, S.S.P. Parkin, Chiral spin torque arising from proximity-induced Magnetization, Nat. Commun. 5 (2014) 1.
[14] W. Zhang, M.B. Jungfleisch, W. Jiang, Y. Liu, J.E. Pearson, S.G.E. te Velthuis, A. Hoffmann, Reduced spin-Hall effects from magnetic proximity, Phys. Rev. B 91 (2015), 115316.
[15] M. Caminale, A. Ghosh, S. Auffret, U. Ebels, K. Ollefs, F. Wilhelm, A. Rogalev, W. E. Bailey, Spin pumping damping and magnetic proximity effect in Pd and Pt spin-sink layers, Phys. Rev. B 94 (2016), 014414.
[16] D.-O. Kim, K.M. Son, Y. Choi, B.-C. Min, J.-S. Kim, J.W. Choi, D.R. Lee, Asymmetric magnetic proximity effect in a Pd/Co/Pd trilayer system, Sci. Rep. 6 (2016) 25391.
[17] A.M. Gonçalves, F. Garcia, H.K. Lee, A. Smith, P.R. Soledade, C.A.C. Passos, M. Costa, N.M. Souza-Neto, I.N. Krivorotov, L.C. Sampaio, I. Barsukov, Oscillatory interlayer coupling in spin Hall systems, Sci. Rep. 8 (2018) 2318.
[18] S. Frota-Pessôa, A.B. Klautau, S.B. Legoas, Influence of interface mixing on the magnetic properties of Ni/Pt multilayers, Phys. Rev. B 66 (2002), 132416.
[19] A. Al-Zubi, G. Bihlmayer, S. Blügel, Magnetism of 3d transition-metal monolayers on Rh(100), Phys. Rev. B 83 (2011), 024407.
[20] M.M. Sigalas, D.A. Papaconstantopoulos, Calculations of the total energy, electron-phonon interaction, and Stoner parameter for metals, Phys. Rev. B 50 (11) (1994) 7255–7261.
[21] F. Wilhelm, P. Poulopoulos, G. Ceballos, H. Wende, K. Baberschke, P. Srivastava, D. Benea, H. Ebert, M. Angelakeris, N.K. Flevaris, D. Niarchos, A. Rogalev, N. B. Brookes, Layer-resolved magnetic moments in Ni/Pt multilayers, Phys. Rev. Lett. 85 (2) (2000) 413–416.
[22] Y. An, L. Duana, T. Liuc, Z. Wuc, J. Liua, Structural and magnetic properties of Pt in Co/Pt multilayers, Appl. Surf. Sci. 257 (2011) 7427–7431.
[23] M. Suzuki, H. Muraoka, Y. Inaba, H. Miyagawa, N. Kawamura, T. Shimatsu, H. Maruyama, N. Ishimatsu, Y. Isohama, Y. Sonobe, Depth profile of spin and orbital magnetic moments in a subnanometer Pt film on Co, Phys. Rev. B 72 (2005), 054430.
[24] A. Lehnert, S. Dennler, P. Błoński, S. Rusponi, M. Etzkorn, G. Moulas, P. Bencok, P. Gambardella, H. Brune, J. Hafner, Magnetic anisotropy of Fe and Co ultrathin films deposited on Rh(111) and Pt(111) substrates: an experimental and first-principles investigation, Phys. Rev. B 82 (2010), 094409.
[25] G. van der Laan, A.I. Figueroa, X-ray magnetic circular dichroism—A versatile tool to study magnetism, Coord. Chem. Rev. 277–278 (2014) 95–129.
[26] N. Jaouen, J.M. Tonnerre, D. Raoux, E. Bontempi, L. Ortega, M. Müenzenberg, W. Felsch, A. Rogalev, H.A. Dürr, E. Dudzik, G. van der Laan, H. Maruyama, M. Suzuki, Ce 5d magnetic profile in Fe/Ce multilayers for the α and γ-like Ce phases by x-ray resonant magnetic scattering, Phys. Rev. B 66 (2002), 134420.
[27] M. Magnuson, Induced magnetism at the interfaces of a Fe/V superlattice investigated by resonant magnetic x-ray scattering, J. Magn. Magn. 422 (2017) 362–366.
[28] L.J. Zhu, D.C. Ralph, R.A. Buhrman, Irrelevance of magnetic proximity effect to spin-orbit torques in heavy-metal/ferromagnet bilayers, Phys. Rev. B 98 (2018), 134406.
[29] J. Bartolomé, L.M. García, F. Bartolomé, F. Luis, R. López-Ruiz, F. Petroff, C. Deranlot, F. Wilhelm, A. Rogalev, P. Bencok, N.B. Brookes, L. Ruiz, J. M. González-Calbet, Magnetic polarization of noble metals by Co nanoparticles in M-capped granular multilayers (M=Cu, Ag, and Au): An x-ray magnetic circular dichroism study, Phys. Rev. B 77 (2008), 184420.
[30] T. Ohkochi, N. Hosoito, K. Mibu, H. Hashizume, Induced magnetic polarization in Cu layers of Gd/Cu multilayers studied by X-ray magnetic circular dichroism, Phys. Soc. Jpn. 73 (2004) 2212–2218.
[31] P. Swaminathan, R.A. Rosenberg, G.K. Shenoy, J.S. Palmer, J.H. Weaver, Induced magnetism in Cu nanoparticles embedded in Co, Appl. Phys. Lett. 91 (2007), 202506.
[32] S. Amasaki, M. Tokunaga, K. Sano, K. Fukui, K. Kodama, N. Hosoito, Induced spin polarization in the Au layers of Fe=Au multilayer in an antiparallel alignment state of Fe magnetizations by resonant X-ray magnetic scattering at the Au L_3 absorption edge, J. Phys. Soc. Jpn. 84 (2015), 064704.
[33] T. Ohkochi, K. Mibu, N. Hosoito, Depth profile of induced spin polarization in Au layers of Fe/Au(001) superlattices by resonant X-ray magnetic scattering, J. Phys. Soc. Jpn. 75 (2006), 104707.
[34] N. Hosoito, K. Kodama, R. Yamagishi, Au spin polarization induced in an Fe/Au (001) multilayer with interlayer exchange coupling from the X-ray energy dependence of resonant X-ray magnetic scattering at the Au L_3 absorption edge, J. Phys. Soc. Jpn. 81 (2012), 064713.
[35] Y. Suzuki, T. Katayama, P. Bruno, S. Yuasa, E. Tamura, Oscillatory magneto-optical effect in a Au (001) film deposited on Fe: experimental confirmation of a spin-polarized quantum size effect, Phys. Rev. Lett. 80 (1998) 5200–5203.
[36] W.A.A. Macedo, W. Keune, E.D. Ellerbrock, Magnetic properties of ultrathin epitaxial fcc-Fe(001) films on Cu(001) and Cu_3Au(001), J. Magn. Magn. Mater. 93 (1991) 552–556.
[37] W.A.A. Macedo, F. Sirotti, A. Schatz, D. Guarisco, G. Panaccione, G. Rossi, Magnetic linear dichroism in photoemission from Fe on $Cu_{84}Al_{16}$(100) and Cu_3Au (100), J. Magn. Magn. Mater. 177–181 (1998) 1262–1264.
[38] M.-T. Lin, J. Shen, W. Kuch, H. Jenniches, M. Klaua, C.M. Schneider, J. Kirschner, Growth, morphology, and crystalline structure of ultrathin Fe films on Cu_3Au(100), Surf. Sci. 410 (1998) 290–311.
[39] F. Baudelet, M.-T. Lin, W. Kuch, K. Meinel, B. Choi, C.M. Schneider, J. Kirschner, Perpendicular anisotropy and spin reorientation in epitaxial Fe/Cu_3Au(100) thin films, Phys. Rev. B 51 (18) (1995) 12563–12578.
[40] B. Roldan Cuenya, M. Doi, S. Löbus, R. Courths, W. Keune, Observation of the fcc-to-bcc Bain transformation in epitaxial Fe ultrathin films on Cu_3Au(001), Surf. Sci. 493 (2001) 338–360.
[41] W.A.A. Macedo, P.L. Gastelois, M.D. Martins, W. Kuch, J. Miguel, M.Y. Khan, Growth, structure, and magnetic properties of epitaxial Ni_xMn_{100-x} single layers and Co/Ni_xMn_{100-x} bilayers on Cu_3Au(100), Phys. Rev. B 82 (2010), 134423.
[42] M.Y. Khan, Y.A. Shokr, W. Kuch, Coupling of pinned magnetic moments in an antiferromagnet to a ferromagnet and its role for exchange bias, Phys.: Condens. Matter 32 (2020), 075801.
[43] A.S. Ponce, S.O. Parreiras, A.A.C. Cotta, G.F.M. Gomes, P. Schio, J.C. Cezar, R. Paniago, P.L. Gastelois, W.A.A. Macedo, Chemical order and magnetic anisotropy in alternate Fe/Co monolayers on Cu_3Au(001), AIP Adv. 8 (2018), 115307.
[44] T. Ohtsuki, T. Kojima, M. Kotsugi, T. Ohkochi, M. Mizuguchi, K. Takanashi, Magnetic domain observation of FeCo thin films fabricated by alternate monoatomic layer deposition, J. Appl. Phys. 115 (2014), 043908.
[45] C.A.F. Vaz, J.A.C. Bland, G. Lauhoff, Magnetism in ultrathin film structures, Rep. Prog. Phys. 71 (2008), 056501.
[46] T. Burkert, L. Nordström, O. Eriksson, O. Heinonen, Giant magnetic anisotropy in tetragonal FeCo alloys, Phys. Rev. Lett. 93 (2004), 027203.
[47] F. Yildiz, F. Luo, C. Tieg, R.M. Abrudan, X.L. Fu, A. Winkelmann, M. Przybylski, J. Kirschner, Strongly enhanced orbital moment by reduced lattice symmetry and varying composition of Fe1xCox alloy films, Phys. Rev. Lett. 100 (2008), 037205.

[48] F. Yildiz, M. Przybylski, X.-D. Ma, J. Kirschner, Strong perpendicular anisotropy in $Fe_{1-x}Co_x$ alloy films epitaxially grown on mismatching Pd(001), Ir(001), and Rh (001) substrates, Phys. Rev. B 80 (2009), 064415.
[49] G. Andersson, T. Burkert, P. Warnicke, M. Björck, B. Sanyal, C. Chacon, C. Zlotea, L. Nordström, P. Nordblad, O. Eriksson, Perpendicular magnetocrystalline anisotropy in tetragonally distorted Fe-Co alloys, Phys. Rev. Lett. 96 (2006), 037205.
[50] A.L. Wysocki, M.C. Nguyen, C.-Z. Wang, K.-M. Ho, A.V. Postnikov, V.P. Antropov, Concentration-tuned tetragonal strain in alloys: application to magnetic anisotropy of $FeNi_{1-x}Co_x$, Phys. Rev. B 100 (2019), 104429.
[51] C. Neise, S. Schönecker, M. Richter, K. Koepernik, H. Eschrig, The effect of chemical disorder on the magnetic anisotropy of strained Fe–Co films, Phys. Status Solidi B 248 (10) (2011) 2398–2403.
[52] Y. Li, F. Zeng, S.S.-L. Zhang, H. Shin, H. Saglam, V. Karakas, O. Ozatay, J. E. Pearson, O.G. Heinonen, Y. Wu, A. Hoffmann, Wei Zhang, Giant anisotropy of gilbert damping in epitaxial CoFe films, Phys. Rev. Lett. 122 (2019), 117203.
[53] T. Hasegawa, T. Niibori, Y. Takemasa, M. Oikawa, Stabilisation of tetragonal FeCo structure with high magnetic anisotropy by the addition of V and N elements, Sci. Rep. 9 (2019) 5248.
[54] Y. Li, F. Zeng, H. Saglam, J. Sklenar, J.E. Pearson, T. Sebastian, Y. Wu, A. Hoffmann, W. Zhang, Optical Detection of phase-resolved ferromagnetic resonance in epitaxial FeCo thin films, IEEE Trans. Magn. 55 (7) (2019) 6100605.
[55] W. Kohn, L.J. Sham, Self-consistent equations including exchange and correlation effects, Phys. Rev. 140 (1965) A1133–A1138.
[56] J.P. Perdew, J.A. Chevary, S.H. Vosko, K.A. Jackson, M.R. Pederson, D.J. Singh, C. Fiolhais, Atoms, molecules, solids, and surfaces: applications of the generalized gradient approximation for exchange and correlation, Phys. Rev. B 46 (1992) 6671–6687.
[57] J.P. Perdew, K. Burke, M. Ernzerhof, Generalized gradient approximation made simple, Phys. Rev. Lett. 77 (1996) 3865–3868.
[58] I. Turek, J. Kudrnovský, K. Carva, Magnetic anisotropy energy of disordered tetragonal Fe-Co systems from ab initio alloy theory, Phys. Rev. B 86 (2012), 174430.
[59] Y. Wei, Y.-Y. Sun, J. Yang, S.-J. Gong, Y.-H. Meng, C.-G. Duan, First-principles investigation of the interface magnetic anisotropy of $Fe/SrTiO_3$, J. Phys.: Condens. Matter 31 (2019), 075803.
[60] K. Lejaeghere, G. Bihlmayer, T. Björkman, P. Blaha, S. Blügel, V. Blum, D. Caliste, I. E. Castelli, S.J. Clark, A. Dal Corso, S. de Gironcoli, T. Deutsch, J.K. Dewhurst, I. Di Marco, C. Draxl, M. Dułak, O. Eriksson, J.A. Flores-Livas, K.F. Garrity, L. Genovese, P. Giannozzi, M. Giantomassi, S. Goedecker, X. Gonze, O. Grånäs, E.K.U. Gross, A. Gulans, F. Gygi, D.R. Hamann, P.J. Hasnip, N.A.W. Holzwarth, D. Iusan, D. B. Jochym, F. Jollet, D. Jones, G. Kresse, K. Koepernik, E. Küçükbenli, Y. O. Kvashnin, I.L.M. Locht, S. Lubeck, M. Marsman, N. Marzari, U. Nitzsche, L. Nordström, T. Ozaki, L. Paulatto, C.J. Pickard, W. Poelmans, M.I.J. Probert, K. Refson, M. Richter, G.-M. Rignanese, S. Saha, M. Scheffler, M. Schlipf, K. Schwarz, S. Sharma, F. Tavazza, P. Thunström, A. Tkatchenko, M. Torrent, D. Vanderbilt, M.J. van Setten, V. Van Speybroeck, J.M. Wills, J.R. Yates, G.-X. Zhang, S. Cottenier, Reproducibility in density functional theory calculations of solids, Science 351 (2016) aad3000.
[61] P.E. Blöchl, Projector augmented-rave method, Phys. Rev. B 50 (1994) 17953–17979.
[62] G. Kresse, D. Joubert, From ultrasoft pseudopotentials to the projector augmented-wave method, Phys. Rev. B 59 (1999) 1758–1775.
[63] G. Kresse, J. Hafner, Ab initio molecular dynamics for open-shell transition metals, Phys. Rev. B 48 (1993) 13115–13118.
[64] G. Kresse, J. Furthmüller, Efficient iterative schemes for ab initio total-energy calculations using a plane-wave basis set, Phys. Rev. B 54 (1996) 11169–11186.
[65] M. Marsman, J. Hafner, Broken symmetries in the crystalline and magnetic structures of g-iron, Phys. Rev. B 66 (2002), 224409.
[66] D. Hobbs, G. Kresse, J. Hafner, Fully unconstrained noncollinear magnetism within the projector augmented-wave method, Phys. Rev. B 62 (2000) 11556–11570.
[67] J.C. Cezar, P.T. Fonseca, G.L.M.P. Rodrigues, A.R.B. de Castro, R. T. Neuenschwander, F. Rodrigues, B.C. Meyer, L.F.S. Ribeiro, A.F.A.G. Moreira, J. R. Piton, The U11 PGM beam line at the Brazilian National Synchrotron Light Laboratory, J. Phys.: Conf. Ser. 425 (2013), 072015.
[68] B.T. Thole, P. Carra, F. Sette, G. van der Laan, X-Ray circular dichroism as a probe of orbital magnetization, Phys. Rev. Lett. 68 (1992) 1943–1946.
[69] P. Carra, B.T. Thole, M. Altarelli, X. Wang, X-ray circular dichroism and local magnetic fields, Phys. Rev. Lett. 70 (1993) 694–697.
[70] S. Dennler, J. Hafner, M. Marsman, J. Morillo, Magnetic doping of 4d transition-metal surfaces: A first-principles study, Magnetic doping of 4d transition-metal surfaces: a first-principles study, Phys. Rev. B 71 (2005), 094433.
[71] J. Stohr, H. Konig, Determination of spin- and orbital-moment anisotropies in transition metals by angle-dependent X-ray magnetic circular dichroism, Phys. Rev. Lett. 75 (1995) 3748–3751.
[72] T. Yokoyama, T. Nakagawa, Y. Takagi, Magnetic circular dichroism for surface and thin film magnetism: Measurement techniques and surface chemical applications, Int. Rev. Phys. Chem. 27 (2008) 449–505.
[73] O. Sipr, J. Minar, H. Ebert, Influence of spin-orbit coupling on the magnetic dipole term T_α, Phys. Rev. B 94 (2016), 144406.
[74] T. Ogushi, T. Shishidou, Anisotropic property of magnetic dipole in bulk, surface, and overlayer systems, Phys. Rev. B 70 (2004), 024412.
[75] A.A.C. Cotta, D.V.P. Massote, G.A.S. Ribeiro, G.C.S. Valadares, R.B. Capaz, E. A. Soares, W.A.A. Macedo, A combined LEED and DFT surface structure determination of $Cu_3Au(001)$: evidence of a surface stacking fault, Surf. Sci. 618 (2013) 167–172.
[76] R. Wu, A.J. Freeman, Limitation of the magnetic-circular-dichroism spin sum rule for transition metals and importance of the magnetic dipole term, Phys. Rev. Lett. 73 (1994) 1994–1997.